Ultra-Low Voltage CMOS Logic Circuits

Luiz A.P.Melek, *Student Member,* Márcio C.Schneider, *Member, IEEE,* and Carlos Galup-Montoro, *Member, IEEE*

***Abstract*— The operation of digital circuits from power supply voltages of the order of 200 mV or less imposes that, in general, MOSFETs are biased in the subthreshold regime, characterized by the exponential relation between control voltages and current. In this tutorial paper we analyze some of the basic building blocks of digital circuits operating in the subthreshold region. We analyze the basic CMOS inverter as regards the voltage transfer characteristic, dynamic behavior, and power dissipation. To reduce the dependence of the drain current on process parameters we show some compensation circuits that adjust the body voltage, with small silicon area penalty. Some properties of the static random access memory (SRAM) are reviewed. Finally, the Schmitt Trigger inverter, which is well suited as a basic building block for ultra-low-voltage operation as a substitute for the standard inverter, is briefly analyzed.**

***Index Terms*—Ultra-low voltage logic, subthreshold, low power, VLSI, static CMOS, SRAM, Schmitt Trigger.**

I. Introduction

In recent years, significant advances toward ultra-low voltage have been achieved, aimed at applications that are energy autonomous or that rely solely on small batteries. Examples of these applications include cell phones, laptops, handhelds and infotainment systems, sensor networks, wearable computing, and biomedical systems [1], [2]. All these applications must save energy and, at the same time, provide intelligence and better performance for costly infrastructure and support in places with difficult access, such as the interior of the human body. Moreover, in the future most electronic devices will include a wireless connection, leading to millions of connected devices [3]. All these devices must capture their own energy, since it is not feasible to use batteries in all of them; nature just cannot absorb all these batteries after their disposal.

In this regard, the reduction in the supply voltage is the fundamental action to increase autonomy. The fundamental limit of the supply voltage in CMOS digital circuits is 36mV at 300K, as determined in [4], [5]. One of the challenges to lower the supply voltage of digital circuits is to compensate the technological parameters variation, mainly the threshold voltage, V_T, of the transistors. Threshold voltage spreading from wafer-to-wafer in a given technology can lead to large variations in the drain current [6]. As a result, the performance of a digital gate can be severely degraded.

Body-biasing has been applied to digital circuits in an attempt to approach the limit of supply voltage and also, to some extent, to compensate for the spreading of process parameters from wafer-to-wafer. Digital circuits were demonstrated to operate from supply voltages of 100 mV, 50 mV, and 85 mV in [6], [7], and [8], respectively. In [9], a 62mV supply voltage is applied to a multiplier based on Schmitt Trigger (ST) structures.

This tutorial is organized as follows. The standard CMOS inverter is analyzed in Section 2. In Section 3, this analysis is extended to the NAND gate. Three circuits are given for proper body biasing to compensate for technological parameters variations in Section 4. In Section 5 we briefly analyze the SRAM memory while Section 6 discusses the application of the Schmitt Trigger inverter for logic circuits. Conclusions are drawn in Section 7.

II. The CMOS Inverter

A. Static Analysis

As the supply voltage is reduced to values lower than the threshold voltage, V_T, of the NMOS and PMOS transistors, the transistors are biased in the subthreshold or weak inversion regime of operation. This regime is characterized by the exponential dependence of the drain current on the gate, drain and source voltages [10], given by (1).

$$I_{DN(P)} = I_{ON(P)} \cdot e^{\frac{V_{GB(BG)} - |V_{TN(P)}| - n_N \cdot V_{SB(BS)}}{n_{N(P)} \cdot \phi_t}} \cdot \left(1 - e^{-\frac{V_{DS(SD)}}{\phi_t}}\right) \quad (1)$$

$I_{ON(P)}$ is a current scaling factor which is dependent on the technology and geometric parameters. V_{GB} and V_{SB} are the gate and source voltages referenced to bulk and V_{DS} is the drain-source voltage. ϕ_t is the thermal voltage and n is the slope factor. The strength or current capability of the transistor is given by

$$I_{N(P)} = I_{ON(P)} \cdot e^{\frac{-|V_{TN(P)}|}{n_{N(P)} \cdot \phi_t}} \quad (2)$$

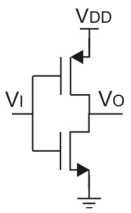

Fig.1: Static CMOS inverter.

This work was funded in part by the Brazilian agencies CAPES and CNPq.

Luiz A.P.Melek. is working towards his PhD at the Federal University of Santa Catarina, Electrical and Electronics Engineering Department, Technology Center, Florianópolis, Santa Catarina, Brazil, 88040-900 (e-mail: betopasini@gmail.com).

Marcio C.Schneider and Carlos Galup-Montoro are with the Federal University of Santa Catarina, Electrical and Electronics Engineering Department, Technology Center, Florianópolis, Santa Catarina, Brazil, 88040-900 (e-mail: marcio.cherem.schneider@gmail.com, carlosgalup@gmail.com).

Considering the standard CMOS inverter in Fig.1, the voltage transfer characteristic (VTC) can be determined from (1). For the sake of simplicity let $n_N=n_P=n$. The static transfer function of the inverter is obtained from

$$I_{DN} = I_{DP} \tag{3}$$

$$I_{ON} \cdot e^{\frac{V_I - V_{TN}}{n \cdot \phi_t}} \cdot \left(1 - e^{-\frac{V_O}{\phi_t}}\right) = I_{OP} \cdot e^{\frac{V_{DD} - V_I - |V_{TP}|}{n \cdot \phi_t}} \cdot \left(1 - e^{-\frac{V_{DD} - V_O}{\phi_t}}\right) \tag{4}$$

$$V_I = \frac{V_{DD}}{2} + \frac{V_{TN} - |V_{TP}|}{2} + \frac{n \cdot \phi_t}{2} \cdot \ln\left(\frac{I_{OP}}{I_{ON}}\right) + \frac{n \cdot \phi_t}{2} \cdot \ln\left(\frac{1 - e^{-\frac{V_{DD} - V_O}{\phi_t}}}{1 - e^{-\frac{V_O}{\phi_t}}}\right) \tag{5}$$

The VTC characterized by equation (5) is dependent on the supply voltage, imbalance of transistor threshold voltages and the ratio of the scaling currents. In the ideal case of NMOS and PMOS transistors with the same strength, i.e. $I_{ON}=I_{OP}$ and $V_{TN}=|V_{TP}|$, the VTC reduces to that given by equation (6).

$$V_I = \frac{V_{DD}}{2} + \frac{n \cdot \phi_t}{2} \cdot \ln\left(\frac{1 - e^{-\frac{V_{DD} - V_O}{\phi_t}}}{1 - e^{-\frac{V_O}{\phi_t}}}\right) \tag{6}$$

The inverter threshold voltage, V_M, is defined as the voltage such that $V_I=V_O$. A first order approximation of V_M derived from (5), given in (7), shows a strong dependence of V_M on the transistors current ratio and threshold voltage mismatch. In the case for which the transistors have the same strength ($I_N=I_P$) then $V_M=V_{DD}/2$. If the NMOS transistor is stronger than the PMOS transistor, $V_M<V_{DD}/2$, whereas if the PMOS transistor is stronger than the NMOS transistor, $V_M>V_{DD}/2$. From (7), it can be noticed that a mismatch in the threshold voltages can be compensated by properly sizing PMOS-NMOS transistors, to obtain $V_M=V_{DD}/2$.

$$V_M \approx \frac{V_{DD}}{2} + \frac{\frac{V_{TN} - |V_{TP}|}{2} + \frac{n \cdot \phi_t}{2} \cdot \ln\left(\frac{I_{OP}}{I_{ON}}\right)}{1 + \left|\frac{dV_I}{dV_O}\right|_{V_O = \frac{V_{DD}}{2}}} \tag{7}$$

$$\left|\frac{dV_O}{dV_I}\right|_{V_O = \frac{V_{DD}}{2}} = \frac{e^{\frac{V_{DD}}{2 \cdot \phi_t}} - 1}{n} \tag{8}$$

The dependence of V_M on the technological parameters is attenuated by the denominator in (7) which has a term that depends on the supply voltage according to expression (8). For n=1, the denominator in (8) is only 1.02 for V_{DD}=200 mV, but it is 1.62 for V_{DD}=50 mV. Thus result is that as the supply voltage is reduced, the influence of the process parameters on V_M is also reduced. For $V_{DD}>4\phi_t$, V_M can be rewritten as

$$V_M = \frac{V_{DD}}{2} + \frac{V_{TN} - |V_{TP}|}{2} + \frac{n \cdot \phi_t}{2} \cdot \ln\left(\frac{I_{OP}}{I_{ON}}\right) \tag{9}$$

The current through the inverter, I_{SC}, can be calculated from (1) and (5) for any input voltage, giving (10) as a result. Particularly, the maximum current, $I_{SC\ MAX}$, is given in (11) when the input voltage is equal to the logic gate threshold voltage, *i.e.* $V_I=V_M$.

$$I_{SC} = \sqrt{I_{ON} \cdot I_{OP}} \cdot e^{\frac{V_{DD} - V_{TN} - |V_{TP}|}{2 \cdot n \cdot \phi_t}} \cdot \sqrt{\left(1 - e^{-\frac{V_O}{\phi_t}}\right) \cdot \left(1 - e^{-\frac{V_{DD} - V_O}{\phi_t}}\right)} \tag{10}$$

$$I_{SC\,MAX} = \sqrt{I_{ON} \cdot I_{OP}} \cdot e^{\frac{V_{DD} - V_{TN} - |V_{TP}|}{2 \cdot n \cdot \phi_t}} \cdot \left(1 - e^{-\frac{V_{DD}}{2 \cdot \phi_t}}\right) \tag{11}$$

Fig.2 shows the VTC and the drain current of the inverter for different supply voltages, $I_{ON}=I_{OP}$=1nA, n=1 and $V_{TN}=|V_{TP}|$=0.3V. It can be noted that as the supply voltage is reduced, the output of the inverter does not fully reach the supply rails. As an example, for V_{DD}=50mV, the output is 46.6mV when the input is 0V, and 3.4mV when the input is 50mV. Practical values can be even worse since the slope factor of the transistors, n, is generally greater than the unity.

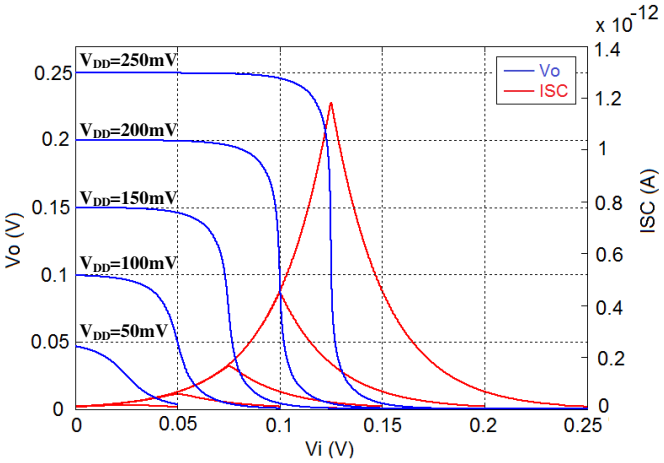

Fig.2: Inverter voltage and current transfer characteristics.

The minimum operating supply voltage of the inverter and any CMOS static logic gate must be at least equal to unity, *i.e.*

$$\left|\frac{dV_O}{dV_I}\right|_{V_O = \frac{V_{DD}}{2}} = 1 \tag{12}$$

for correct binary signal interpretation [4]. Using (12) together with (8) for n=1, we can readily find that

$$V_{DD\,\min} = 2\phi_t \ln(2) = 36\text{mV at } 300\text{K} \tag{13}$$

which is the result presented in [4] and [5].

B. *Dynamic Analysis*

The rise and fall times of the inverter, T_{LH} and T_{HL}, respectively, are determined from the circuits shown in Fig.3. $T_{LH(HL)}$ is the time needed to charge (discharge) the output node between 10% and 90% (90% and 10%) of V_{DD}. Applying a step to the input, the values of T_{HL} and T_{LH} are [11]

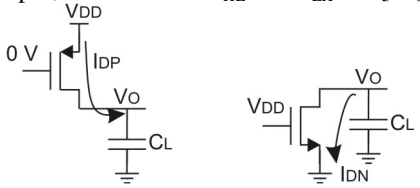

Fig.3: (a) Charging C_L; (b) Discharging C_L.

$$I_{DN(P)} = \mp C_L \cdot \frac{dV_O}{dt} \tag{14}$$

$$I_{ON(P)} \cdot e^{\frac{V_{DD}-|V_{TN(P)}|}{n_{N(P)}\cdot\phi_t}} \cdot \left(1 - e^{-\frac{V_O}{\phi_t}}\right) = \mp C_L \cdot \frac{dV_O}{dt} \tag{15}$$

$$t_{HL(LH)} = \frac{0.8 \cdot V_{DD} + \phi_t \cdot \ln\left(\dfrac{1 - e^{-\frac{0.9\cdot V_{DD}}{\phi_t}}}{1 - e^{-\frac{0.1\cdot V_{DD}}{\phi_t}}}\right)}{I_{ON(P)} \cdot e^{\frac{V_{DD}-|V_{TN(P)}|}{n_{N(P)}\cdot\phi_t}}} \cdot C_L \tag{16}$$

C. Power Dissipation

Generally, the power dissipation in a circuit can be divided into dynamic and short-circuit power, both dependent on the switching frequency, and static power, which is independent of the frequency.

The dynamic power is associated with the energy dissipated in the transistors to charge and discharge the load capacitance. It is calculated as the average energy transferred from the power supply to the load, in a full switching cycle, *T*. In the first half-cycle, a charge *Q,* eq. (17), provided by the supply is used to raise the output capacitor voltage, through the PMOS transistor, as shown in Fig.3 (a). In the second half-cycle, the capacitor is discharged through the NMOS transistor, as Fig.3 (b) shows. The result is an average current, I_{AVG}, through the power supply, as given by (18). The dynamic power, P_{DYN}, is then calculated as the product of the average current and supply voltage, from (17) to (19), and is valid for the case in which the capacitor is fully charged to V_{DD} and discharged to *GND*, which is a rough approximation for very low supply voltages.

$$Q = C_L \cdot V_{DD} \tag{17}$$

$$\frac{Q}{T} = I_{AVG} = C_L \cdot V_{DD} \cdot f \tag{18}$$

$$P_{DYN} = I_{AVG} \cdot V_{DD} = C_L \cdot V_{DD}^2 \cdot f \tag{19}$$

The short-circuit power, P_{SC}, is due to the simultaneous conduction of the PMOS and NMOS transistors during a transition. The short-circuit current, I_{SC}, given by (10) for any voltage, as shown in Fig.4, is maximum when V_I=V_M. The short-circuit power P_{SC} is given by

$$P_{SC} = V_{DD} \cdot \frac{1}{T} \cdot \int I_{SC} \cdot dt \tag{20}$$

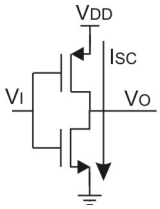

Fig.4: Short-circuit current

The static power, P_{ST}, in (21) is due to the transistors dissipation when they are supposedly in the off state. Even when the transistors are off, a small leakage current, $I_{LKN(P)}$, flows as shown in Fig.5. I_{LK}, derived from (1), is given in (22).

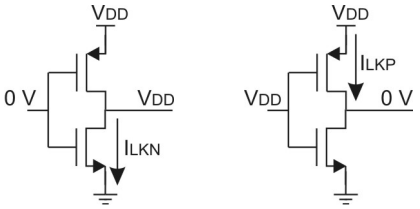

Fig.5: (a) NMOS leakage; (b) PMOS leakage.

$$P_{STN(P)} = I_{LKN(P)} \cdot V_{DD} \tag{21}$$

$$I_{LKN(P)} = I_{ON(P)} \cdot e^{\frac{-|V_{TN(P)}|}{n_{N(P)}\cdot\phi_t}} \tag{22}$$

In all cases, the dynamic, short-circuit and static power, which are of major concern in low power circuits, are greatly reduced with supply voltage reduction. Dynamic power is the most affected since it is dependent on the square of V_{DD}.

III. The NAND Gate

The analysis carried out for the inverter input-output relation, which resulted in (5) and (7), can be extended to more complex logic gates such as the NAND gate, which is shown in Fig.6. The output changes state for one of the two following events. In the first one, labeled as (a) in (23), one of the inputs, e.g. V_A, changes whereas the other is held constant at (or close to) V_{DD}. In the second case, labeled as (b) in (23), both inputs vary simultaneously, *i.e.* $V_A \equiv V_B$. In this case, the NAND gate is equivalent to an inverter with a P-channel transistor equivalent to the parallel association of P_1 and P_2 and an NMOS transistor equivalent to the series association of N_1 and N_2. The equivalent strength, I_{EQ}, of the series/parallel associations of the NAND transistors is in (23).

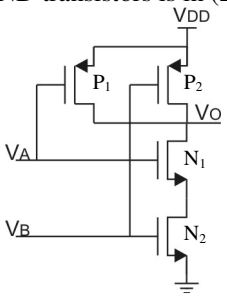

Fig.6: The 2-input NAND gate.

$$\left.\begin{aligned} I_{EQ,P} &= I_P \text{ and } I_{EQ,N} = I_N && \text{(a)} \\ I_{EQ,P} &= I_P \cdot 2 \text{ and } I_{EQ,N} = I_N/2 && \text{(b)} \end{aligned}\right\} \tag{23}$$

The relations in (23) reveal that the threshold V_M of the logic gate depends on whether one input varies alone or both vary together. Fig.7 shows the VTC of the NAND gate obtained from equation (5) with conditions (a) and (b) in (23) for V_{DD}=150mV.

The series/parallel association of transistors can be extended to logic gates with more inputs without any

degradation in the output voltage due to the transistor stacking.

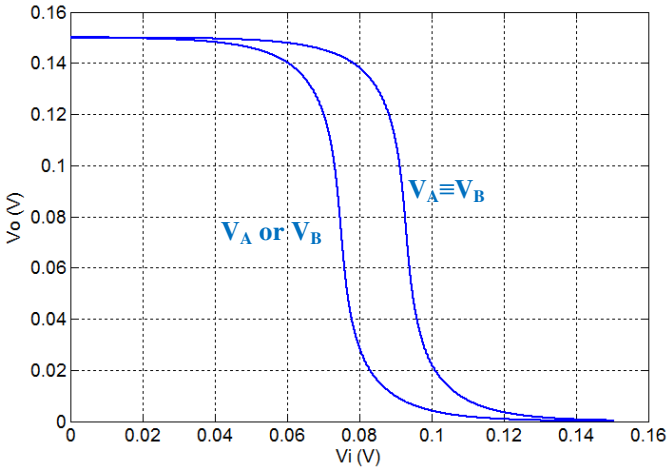

Fig.7: NAND VTC when only one input varies (V_A or V_B) or when both vary together ($V_A \equiv V_B$).

IV. Body Bias Compensation

The transistor drain current in the subthreshold region, equation (1), is very sensitive to V_T. Typical variations of V_T from batch to batch can lead to considerable current variation. Fig.8 shows the simulation of the typical current $I_{DN(P)}$ transfers versus the gate-to-source voltage with nominal threshold voltages close to 500mV and ±30mV variations, for a 180nm technology. Current can vary by as much as a factor of five in the exponential region.

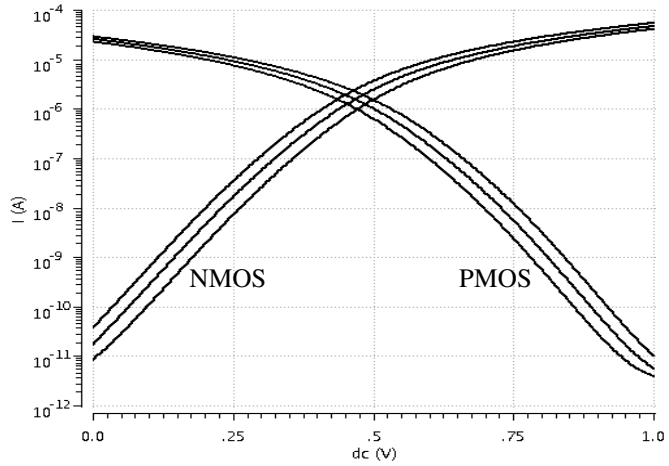

Fig.8: NMOS and PMOS drain current.

Variations in the process parameters result in shifts in the voltage transfer characteristic (VTC) of a CMOS inverter, as can be inferred from (7). If the PMOS transistor and the NMOS transistor are well matched, V_M equals $V_{DD}/2$. But for fast NMOS (lower V_T) and slow PMOS (higher V_T) transistors, V_M is less than $V_{DD}/2$; conversely, for slow NMOS (higher V_T) and fast PMOS (lower V_T) transistors, V_M is greater than $V_{DD}/2$. This is exemplified in Fig.9, assuming that the threshold voltages can vary ±30mV around the typical (TT) value. In Fig. 9, the supply voltage is 150mV, FS stands for fast NMOS and slow PMOS transistors, while SF stands for slow NMOS and fast PMOS transistors.

The variation of process parameters also affects the rise and fall times of the inverter, as equation (16) shows. Variations of an order of magnitude in the NMOS or PMOS drain currents result in rise and fall times that also differ by an order of magnitude. This represents a waste of energy since the maximum operating frequency is mostly determined by the higher of the sum of the expected fall and rise times. So, proper techniques must be applied in order to compensate, to some extent, the large variations of the drive currents and, consequently, avoid the waste of energy. Fig.10 shows the transient simulation of the charge and discharge of a load capacitor, C_L=50fF, driven by an inverter with different NMOS and PMOS drain current capabilities, for a supply voltage of 200 mV. The rise and fall times are clearly very different due to the slow NMOS and fast PMOS transistors.

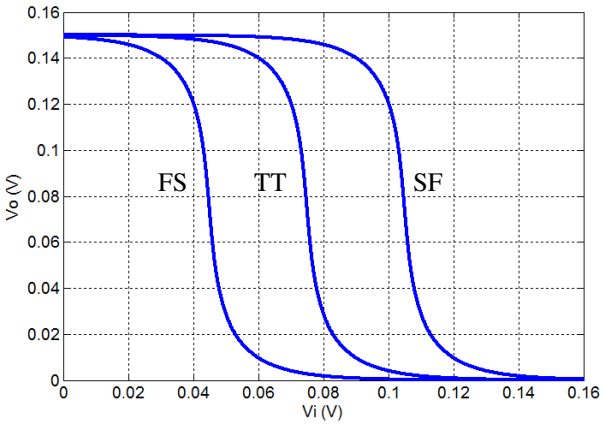

Fig. 9: Inverter VTC under the influence of process parameters variation.

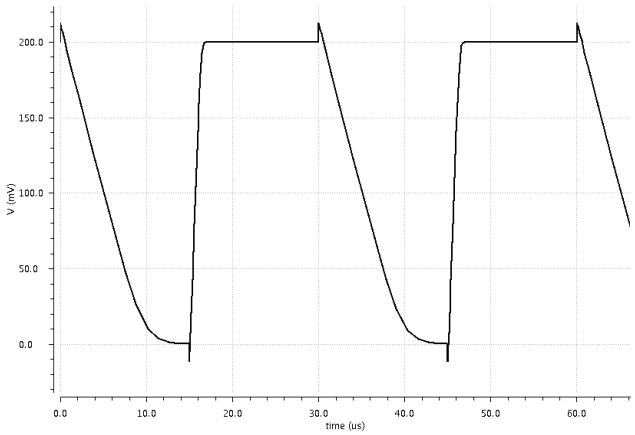

Fig.10: Transient simulation of the charge and discharge of a 50fF load capacitor by an unbalanced CMOS inverter.

Expression (1) also shows that a variation of the source-to-body voltage, V_{SB}, of the transistor affects the drain current. With a proper body voltage, mismatches in the drive current in the NMOS and PMOS can be reduced regardless their sizes and technological parameters. Reverse body-biasing (RBB) is a technique in which the body bias voltage is higher than V_{DD} for the P transistor and lower than GND for the N transistor. This technique is good for leakage current reduction, but has the great inconvenience of the need of bias voltages higher than V_{DD} and lower than GND. Forward body-biasing (FBB)

is another technique in which the body voltages are between GND and V_{DD}. An inverter with body-bias voltages V_{BN} and V_{BP} is shown in Fig.11.

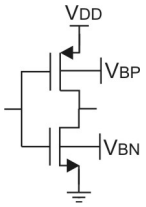

Fig.11: Inverter with body-bias.

In Fig.12, three bias circuits that can be used to compensate for process variations by providing appropriate forward body-bias voltage, V_W, are shown. V_W is a common voltage applied to both NMOS and PMOS transistors of a logic gate. In the three circuits, V_W is a voltage that results from the equalization of the NMOS and PMOS currents. Note that both source-to-bulk parasitic diodes are forward body-biased (FBB), so V_{DD} is limited to sub-1V voltages. Low voltage operation is also recommended to avoid latch-up. The circuit in Fig.12 (a) was proposed in [6] to equalize the "off" currents of the complimentary devices. Two derivations of this circuit were proposed in [11]: the circuit in Fig.12 (b) compensates the "on" or driving currents of the MOSFETs, while the one in Fig.12(c) compensates the currents for an input equal to the gate threshold.

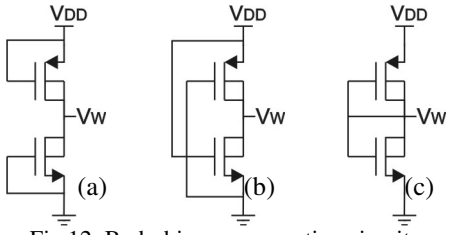

Fig.12: Body-bias compensation circuits
(a) "off" circuit; (b) "on" circuit; (c) "midway" circuit.

The analysis of the circuits in Fig.12 is straightforward. Noting that

$$I_{DP} = I_{DN} \tag{24}$$

the value of V_W for the circuit in Fig.12(c) can be determined from (1), resulting in

$$I_{OP} \cdot e^{\frac{0-|V_{TP}|-n_P\cdot(V_W-V_{DD})}{n_P\cdot\phi_T}} = I_{ON} \cdot e^{\frac{0-V_{TN}-n_N\cdot(0-V_W)}{n_N\cdot\phi_T}} \tag{25}$$

Solving (25) for V_W gives:

$$V_W = \frac{V_{DD}}{2} + \frac{V_{TN}}{2\cdot n_N} - \frac{|V_{TP}|}{2\cdot n_P} + \frac{\phi_T}{2}\ln\left(\frac{I_{OP}}{I_{ON}}\right) \tag{26}$$

The body-bias compensation voltage, V_W, given in (26) is similar to the threshold voltage V_M of the inverter given by (9). This is due to the fact that the inverter shown in Fig.1 and the circuit in Fig.12(c) are similar. The similarity comes from the fact that the inverter threshold voltage is determined by making V_I=V_O, *i.e.* by shorting the output and input nodes, exactly as done in Fig. 12 (c). The main difference between the inverter and the circuit in Fig. 12 (c) is that the MOSFETs in the latter circuit have their bodies connected to the drain, whereas in the former the bodies are connected to the source.

As an example of the effect of the bias voltage, a comparison between transient simulations of an inverter without body-bias (NBB) and with forward body-bias compensation (FBB) from the circuit in Fig.12(c) is shown in Fig. 13 for a supply voltage of 200mV. Clearly, the rise and fall times of the inverter with body-bias are closer than the ones of the inverter without body-bias. The simulation also shows another benefit of the FBB: the rise and fall times are faster than without body-bias, leading to improved performance at the same supply voltages; at the price of the same static power dissipation, faster clocks can be used.

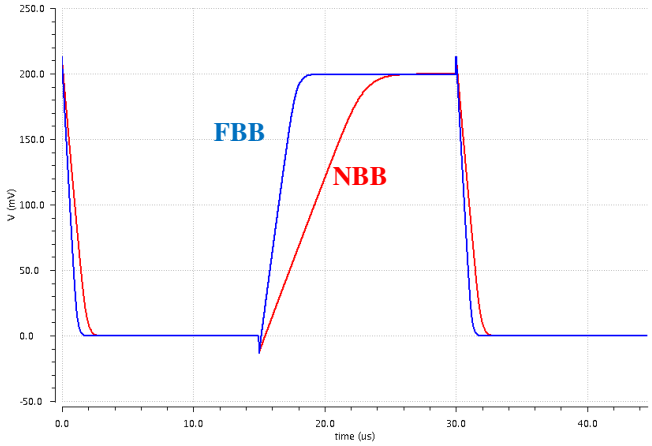

Fig.13: Inverter transient with (FBB) and without body-biasing (NBB).

V. THE SRAM

The six-transistor cell composed of 2 cross-coupled inverters, the so-called bistable latch, and 2 switches, as shown in Fig.14, is the standard SRAM bitcell. Each bitcell is selected by its corresponding wordline WL. The requirement of this cell is such that the resistance of the pass transistors connected to the bitlines BL and BR must be sufficiently low to allow correct writing but high enough to avoid stored data to flip during reading mode. For example, during a read operation, the stored data can flip from '0' to '1' due to the voltage divider formed by the pass transistor and the NMOS transistor of the inverter, since both bitlines are precharged to V_{DD}. With proper sizing this can be avoided, but under process, voltage and temperature (PVT) variations, this requirement may be challenging and may result in different failure modes such as read, hold, write and access time failures. Additionally, the SRAM is much more prone to failures for low supply voltages.

The VTC of the first inverter of the SRAM latch in Fig.14 and the inverted VTC of the second inverter, when the horizontal and vertical axes are permuted, forms the butterfly plots shown in Fig.15 for three different supply voltages. For higher voltages, the curves intercept at two stable points (open circle), V_H and V_L, and one metastable point (closed circle). As the supply voltage gets lower, and so the maximum gain of the inverters, the two stable points get closer to the metastable point and can even become indistinguishable from it, resulting in low output voltage swing (given by the difference between V_H and V_L) and in logic failure [13]. Fig. 16 shows the values

of V_H and V_L as a function of the supply voltage for the case where the PMOS and NMOS transistors have the same strength, with n=1.5. In this case, there is only one stable point for V_{DD}<50 mV, *i.e.* the SRAM is ineffective. For higher supply voltages, there are two stable points, V_H and V_L, and one metastable point, V_M. In this case, the SRAM is effective as long as V_H and V_L are distinguishable by the read circuit.

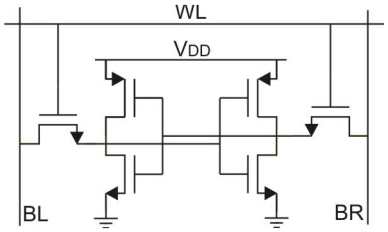

Fig. 14: Classical 6T SRAM.

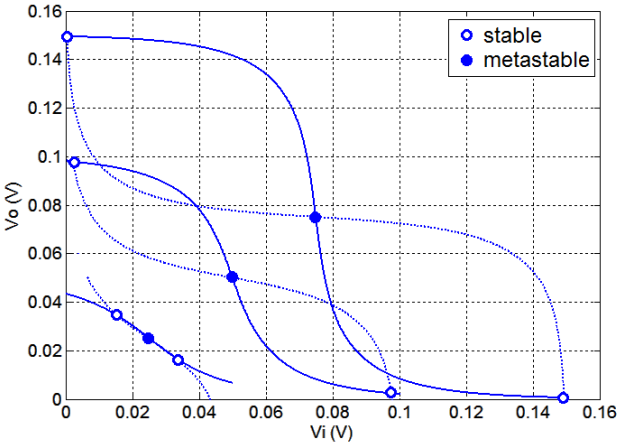

Fig. 15: SRAM latch butterfly plot – n=1.5.

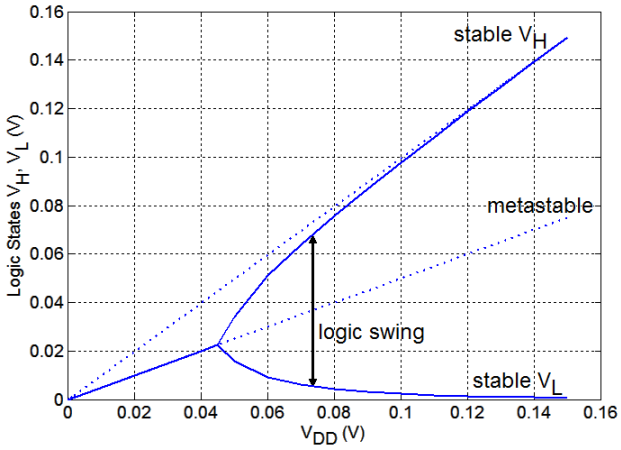

Fig.16 SRAM latch output logic states – n=1.5.

VI. Schmitt Trigger Based Logic

The classical 6-transistor Schmitt Trigger (ST) inverter shown in Fig.17(a), is a common digital circuit that can be used either as an input filter to de-bounce signals or in SRAM memories, as shown in Fig.17(b) [12], or as part of analog oscillators due to the hysteresis effect. Although the ST operation has been analyzed for strong inversion [14], [15], little effort has been directed toward modeling it in weak inversion. In [9], an analytical expression of the internal node potential, V_X, is derived to compare the leakage currents of the ST and the standard inverter.

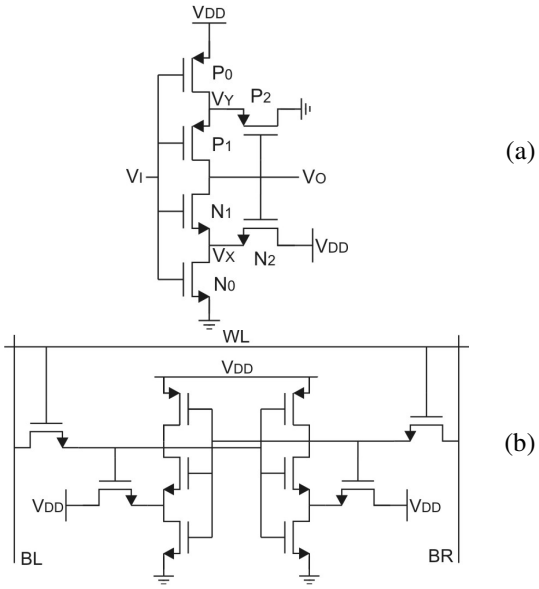

Fig. 17: (a) 6-T Schmitt Trigger; (b) SRAM based on the ST [12].

The main topological difference of the ST as compared to the conventional CMOS inverter is the inclusion of two internal nodes in the NMOS and PMOS networks, which are connected to the positive feedback transistors P_2 and N_2 controlled by the output voltage, V_O. These transistors are responsible for the hysteresis effect when operated with supply voltages higher than around 100mV [9]. For supply voltages below this level, hysteresis is not present. Actually, a lack of hysteresis is preferable for V_{DD} minimization [7], [12] in order to maximize SNM. The VTC for a supply voltage of 120mV is shown in Fig. 18. One of the benefits of the ST is that although it does not reduce leakage, it shifts the leakage path so that the output voltage is not loaded [9]. In this sense, when the input is at GND and the output is high, N_2 pulls V_X to a high potential. Thus, the gate-to-source voltage of N_1 becomes negative and its drain to source voltage is near zero. For the two reasons above, the current flowing in N_1 is greatly reduced and output voltage deviation is lower [9].

For an optimized behavior [8], the corresponding PMOS and NMOS transistors must have the same current strength. Thus, N_0 and P_0, N_1 and P_1, and N_2 and P_2 in Fig.17(a) have the same current strength, which are labeled as I_0, I_1 and I_2, respectively. The node voltages, V_Y, V_X and V_O are determined by the KCL and the application of (1) to the pull-up and pull-down networks gives

$$I_{DN0} = I_{DN1} + I_{DN2} \tag{27}$$

$$I_0 \cdot e^{\frac{V_I}{\phi_t}} \cdot \left[1 - e^{-\frac{V_X}{\phi_t}}\right] = I_1 \cdot e^{\frac{V_I}{\phi_t}} \cdot \left[e^{-\frac{V_X}{\phi_t}} - e^{-\frac{V_O}{\phi_t}}\right] + I_2 \cdot e^{\frac{V_O}{\phi_t}} \cdot \left[e^{-\frac{V_X}{\phi_t}} - e^{-\frac{V_{DD}}{\phi_t}}\right] \tag{28}$$

Solving (28) for V_X results

$$e^{\frac{V_X}{\phi_t}} = \frac{I_0 + I_1 + I_2 \cdot e^{\frac{V_O - V_I}{\phi_t}}}{I_0 + I_1 \cdot e^{-\frac{V_O}{\phi_t}} + I_2 \cdot e^{\frac{V_O - V_I}{\phi_t}} \cdot e^{-\frac{V_{DD}}{\phi_t}}} \quad (29)$$

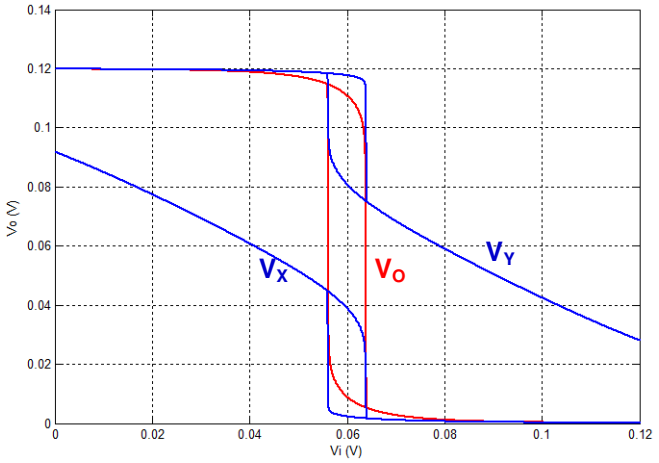

Fig. 18: ST VTC for V_{DD}=120mV.

The Schmitt Trigger (ST) based SRAM in Fig.17(b) requires no architectural changes and shows better read static noise and built-in process variation tolerance [12] if compared to the SRAM based on the conventional inverter. The ST inverter increases or decreases the trip point of the cell, due to the hysteresis effect of the ST, depending on the direction of the input transition, resulting in higher SNM. So, the ST is used to reduce unexpected flips in the stored data.

VII. Conclusion

In this tutorial, the basic logic gates aimed at ultra-low voltage operation working principles were summarized. These gates need additional schemes to compensate for process parameters variations, being the application of a body-bias voltage one of the most commonly used compensation method. As an alternative, the Schmitt Trigger inverter was reviewed and interesting aspects of its operation in weak inversion were shown. Due to its features, the Schmitt Trigger is a promising circuit for a broad range of ultra-low-voltage applications.

References

[1] M. Alioto, "Ultra-low power VLSI circuit design demystified and explained: A Tutorial", IEEE Transactions on Circuits and Systems I – Regular Papers, vol. 59, no.1, Jan 2012.

[2] A. Cardoso, L. de Carli, C. Galup-Montoro, M.C.Schneider, "Analysis of the rectifier circuit valid down to its low-voltage limit", IEEE Transactions on Circuits and Systems I – Regular Papers, vol. 59, no.1, Jan 2012.

[3] J.Rabaey, "The swarm: what it means to Microsystems education," IEEE Microelectronic systems Education (MSE), San Diego, Jun 2011, http://www.mseconference.org/SwarmKeynoteMSE11.pdf.

[4] J. D. Meindl and J. A. Davis, "The fundamental limit on binary switching energy for terascale integration (TSI)," IEEE Journal of Solid-State Circuits, vol. 35, no. 11, pp. 1515-1516, Oct 2000.

[5] R. M. Swanson and J. D. Meindl, "Ion-implanted complementary MOS transistors in low-voltage circuits," IEEE Journal of Solid-State Circuits, vol. 7, no. 2, pp. 146-153, Apr 1972.

[6] A. Bryant et al., "Low-power CMOS at Vdd=4kT/q", Device Research Conference, 2001.

[7] M. Hwang, "Supply-voltage scaling close to the fundamental limit under process variations in nanometer technologies", IEEE Transactions on Electron Devices, vol.58, no.8, Aug 2011.

[8] K. Roy, J.Kulkarni,M. Hwang, "Process-tolerant ultralow voltage digital subthreshold design", IEEE Topical Meeting on Silicon Monolithic Integrated Circuits in RF Systems, Jan 2008.

[9] N. Lotze, Y. Manoli, "A 62mV 0.13um CMOS standard-cell-based design technique using Schmitt-Trigger logic", IEEE Jounal of Solid-State Circuits, vol. 47, no. 1, pp 47-60, Jan 2012.

[10] M.C.Schneider and C.Galup-Montoro, "CMOS Analog Design Using All-Region MOSFET Modeling", 1st Edition, Cambridge University Press, 2010, pp. 51-53.

[11] L.A.P.Melek, M.C.Schneider, C.Galup-Montoro, "Body-bias compensation technique for subthreshold CMOS static logic gates", in Proceedings of 17th Symposium on Integrated Circuits and Systems Design (SBCCI), pp. 267-272, 2004.

[12] J. Kulkarni, K. Kim, K. Roy, "A 160mV, fully differential, robust Schmitt Trigger based sub-threshold SRAM", Low Power Electronics and Design, ISLPED, 2007.

[13] E. Vittoz, "Weak inversion for ultimate low-power logic," in *Low-Power Electronics Design*, CRC Press, 2005, pp.16.1-16.18.

[14] B. Dokic, "CMOS Schmitt triggers", IEEE Proceedings, vol. 131, no.5, Oct 1984.

[15] I. Filanovsky, H. Baltes, "CMOS Schmitt Trigger design", IEEE Transactions on Circuits and Systems-I: Fundamental Theory and Applications, vol.41, no.1, Jan 1994.

Luiz Alberto Pasini Melek (M'13) studied Electrical Engineering at the Federal University of Paraná (UFPR), Curitiba, Brazil. He received the M.S. degree in 2004 from the Federal University of Santa Catarina (UFSC). He is currently working towards the PhD degree at the UFSC. His main interests are ultra-low voltage digital circuits and mixed-signal circuits for VLSI.

Márcio Cherem Schneider (M'90) received the B.E. and M.S. degrees in electrical engineering from the Federal University of Santa Catarina (UFSC), Brazil, in 1975 and 1980, respectively, and a Ph.D. degree in electrical engineering from University of São Paulo, São Paulo, Brazil, in 1984.

In 1976, he joined the Electrical Engineering Department of UFSC, where he is now a Professor. In 1995, he spent a one-year sabbatical at the Electronics Laboratory of the Swiss Federal Institute of Technology, Lausanne. In 1997 and 2001, he was a Visiting Associate Professor at Texas A&M University.

Carlos Galup-Montoro (M'89) studied engineering sciences at the University of the Republic, Montevideo, Uruguay, and electronic engineering at the National Polytechnic School of Grenoble (INPG), France. He received the M.S. degree in engineering degree in electronics in 1979 and the Ph.D. degree in 1982, both from INPG.

From 1982 to 1989 he worked at the University of São Paulo, Brazil. Since 1990, he has been a member of the Electrical Engineering Department, Federal University of Santa Catarina, Florianópolis, Brazil, where he is now a

Professor. From August 1997 to February 1998 he was a Research Associate with the Analog Mixed Signal Group, Texas A&M University. From August 2008 to July 2009 he was a visiting scholar at the University of California, Berkeley.